International Journal of Scientific and Technical Research in Engineering (IJSTRE)
www.ijstre.com Volume 4 Issue 5 ǁ Sep-Oct 2019.
ISSN: 2581-9941

Ellipsometric investigation of annealing effect on the optical properties of WO_3/Ag/WO_3 multilayer

K. Ahmadi
Material and Energy Research Center (MERC), Tehran, Iran.

Abstract: *Multilayer films produced by using electron-beam evaporation. The thickness of WO_3 layers fixed at 40 nm, while Ag layer thickness varied in 10, 12 and 14 nm. Annealing carried out at 300℃ for 1 hour after WO_3 layer deposition. The effects of annealing on the structural and optical properties of WO_3/Ag/WO_3 examined. Ellipsometry spectroscopy executed in the wavelength range from 300 to 900 nm in air at angle ϕ = 70° of radiation incidence with the normal to the surface. Spectroscopy intuitively shows the thicknesses of the films and interdiffusion between layers. We notice there is almost no interfering between two WO_3 /Ag layers with 12 and 14 nm Ag thickness when silver deposited on the annealed WO_3 layer. Individual layers examined using atomic force microscopy (AFM) and revealed that a smoother layer can achieve after annealing. UV-visible spectroscopy showed, in addition of Ag film thickness, annealing of the first WO_3 layer improves the transparency in the visible region. The heat mirrors performance assessed on the principle of their optical behavior and 14 nm thickness of Ag film found to be the ideal with a transmittance of 94% in the wavelength of 550 nm.*

Keywords*: Ellipsometery; Annealing; Heat mirror; WO_3/Ag/WO_3; Multilayer.*

I. Introduction

Transparent heat mirrors divided into different classes characterized by their application or construction. Considering applications, two groups exist: 1. Mirrors which transmit visible light and in the ideal case reflect over the total infrared heat spectrum. The category contains all present applications related to energy conservation and personal protection [1], light bulb envelopes [2], furnace windows [3], welder and laser goggles, astronaut helmets. 2. Mirrors are transparent to visible and near -infrared light and reflective only beyond the near -infrared transmission cut -off. This covers, heat mirrors comprise solar heat collector covers and window coatings for the passive solar heating of building applications. Some of these applications are still in an early development stage. Three approaches have been suggested for the construction of transparent heat mirrors. First tendency, conducting microgrids, does not necessarily depend on a substrate. In two other methods, a transparent substrate is crucial, either covered by a single -layer or a multi -layer coating. Multilayer films include dielectric overcoated metals such as ZnS/metal/ZnS, Bi_2O_3/Au/Bi_2O_3, and TiO_2/Ag/TiO_2.

A transparent heat mirror (THM) provides transparency in a visible light in the $0.4 < \lambda < 0.7$ μm wavelength range, while can reflect IR thermal radiation in the $0.7 < \lambda < 3$ μm wavelength interval. THMs have a great number of applications in many fields, namely energy efficiency, solar photovoltaic conversion and solar heating [4]. Metallic thin film is a main material using in fabricating of THM due to their high free-electron density, which lead to high reflectance in the visible and infrared ranges [5]. In principle, if the refractive index of the single layer metal film is zero the most transparency in the visible range can be achieved [6]. In this case the only loss attributed to the absorption, $4\pi kd/\lambda$ where k is the extinction coefficient, d is the thickness of the thin film and λ is the wavelength of the incident light. This reflective loss happens owing to the fact that the coefficient reflectance of the two interfaces is in opposite phases which results in destructive interference [7]. No perfect metal with n=0 exist, so due to undesirable short wavelength absorption reported for the metals like Ag, Au and Cu at $\lambda < 0.5\,\mu m$ and at $\lambda \approx 0.8$ μm for Al [8], silver with both the lowest refractive index n and absorption in the visible region has been chosen in this work. Nevertheless, when metal deposited on the dielectric substrates like glass it experiences a particular process known as growth stages, including metal nuclei, metal islands, large-scale coalescence and uniform thin film [8]. Thinner metal films vulnerable to form island-like structure which is regarded as a serious limitation on the heat mirror performance [9]. Uniform metal thin film sandwiched between two dielectric layers makes these layers are heavily reflectance at IR region and antireflective in the visible region. The dielectric/metal/dielectric (DMD) system, therefore able to be more transparent in the visible region. The effective thickness of the Ag reduced when a diffusion process occurs [10]. Furthermore, because of oxidation and corrosion single metal film does not present durability and stability required in producing the heat mirrors [11]. Here we show that annealing the first WO_3 deposited layer has a significant impact on both achieving the effective thickness of the layers and the selectivity of the DMD system.

II. Experimental technique

Film deposition on a glass substrate is a delicate process. The glass substrates cleaned by ultra-sonication in propanol, acetone and deionized water for 8 minutes, afterwards they dried by blowing high purity N_2 gas. Materials powders of WO_3 (Fluka, code 95410) and Ag (Fluka, code 85130 purity 99.99%) used. The WO_3 powder out-gassed before starting evaporation. Then WO_3, Ag and WO_3 films prepared under vacuum pressure of 4×10^{-3} Pa. The evaporation rates were around 0.1 nm/s and 1 nm/s for WO_3 and Ag, respectively. WO_3/Ag/WO_3 deposited using electron-beam evaporation (Edwards auto 360). The thickness of the layers and the evaporation rate controlled by a quartz crystal thickness monitor and Ellipsometry analyses. Three different sets of D/M/D systems with a different silver layer thickness engineered and compared with each other. The first layer of WO_3 annealed samples A_1, B_1 and C_1, compared to as deposited samples A, B and C. Every set labeled by their nominal thickness as follows:

Sample A and A_1: WO_3(40 nm)/Ag (10 nm)/WO_3(40 nm)
Sample B and B_1: WO_3(40 nm)/Ag (12 nm)/WO_3 (40 nm)
Sample C and C_1: WO_3(40 nm)/Ag (14 nm)/WO_3(40 nm)

WO_3 film annealed at 100, 200, 300 and 400 ℃ for an hour in the air. Stylus profilometer (Taylor Hobson) used to measure the thickness of the films. Ellipsometry analyses performed to measure optical constant and surface morphology of the films using Sentech 800 instrument, and Spectra Ray software to analyze data. The Surface morphology and roughness also examined by Atomic Force Microscopy (AFM) using a Park Scientific instrument applying in non-contact mode. Optical transmittance measured by UV-Visible spectrophotometer (Perkinelmer, Lambda 25 Spectrometer) in the range 300-1100 nm.

2.1. Models for ellipsometry analysis:

Table 1 illustrates the models applied to exam the films by ellipsometry. The model for WO_3 films described by Tauc-Lorentz model (TL), the model that, applied for dielectric function for both transparent conductive oxides [12] and amorphous materials [13]. The TL uses empirical relation of the Tauc expression for the imaginary part of the dielectric function ($\varepsilon_2(E)$) near the band edge and the Lorentz oscillator.

$$\varepsilon_2(E) = A_T \frac{\left(E - E_g\right)^2}{E^2} \Theta(E - E_g) \quad (1)$$

Where $\Theta(E - E_g)$ is the Heaviside function ($\Theta(E < 0) = 0, \Theta(E \geq 0) = 1$) and E_g is the band gap of the material. The real part of the Tauc-Lorentz (ε_1) can be calculated by a Kramers-Kronig integration of $\varepsilon_2(E)$:

$$\varepsilon_1(E) = \varepsilon_\infty + \frac{2}{\pi} P \int_{E_g}^{\infty} \frac{\xi \varepsilon_2(\xi)}{\xi^2 - E^2} d\xi \quad (2)$$

Where the *P* presents the Cauchy principal part of the integral and normally ε_∞=1.

For inhomogeneous materials and interfaces between layers, the effective medium approximation (EMA) applied to calculate the complex refractive index [14]. Using Bruggeman EMA equation is common in ellipsometry [15] and can be written

$$\sum_{i=1}^{n} f_i \frac{\varepsilon_i - \varepsilon_{eff}}{\varepsilon_i + 2\varepsilon_{ff}} = 0\,, \quad \sum_{i=1}^{n} f_i = 1, \quad (3)$$

Where *n*=2 indicate two components, and ε_i and f_i are the complex dielectric function and the volume fraction of the component *i*, respectively.

The mean square error (MSE) between the fitted model and the measured data by Levenberg-Marquardt regression algorithm. In this manner, the goodness of the fit calculated from the measurement data and for refereeing the validity is achieved. This algorithm delivers 90% confidence limits for the fitting data [15], that lower the MSE.

Table 1. Structural models for WO_3/Ag/WO_3 thin films on substrates of borosilicate glass.

WO_3
EMA
Ag
EMA
WO_3
GLASS

III. Results and discussion

3.1. Ellipsometry analysis

Optical properties and metrology analysis of WO_3/Ag layers studied by use of spectroscopic Ellipsometry. Ellipsometer is a device used for the measurement and evaluation of the thickness and refractive index of very thin films. Ellipsometry analysis obtained, by considering a Cauchy model to represent the borosilicate glass readings and Drude model for the Ag thin film. The MSE value calculated to show the quality of the fitting. Figure 1 shows the measured and best fit ellipsometric data (Ψ, Δ) in the wavelength range from 300 to 900 nm in air at angle ϕ = 70° of radiation incidence with respect to the normal to the surface of WO_3/Ag/WO_3/glass. Table 2 is a list of the thicknesses obtained by model layers of ellipsometry analysis and the MSE value. Figure 2 illustrates the extinction coefficient of Ag thin film calculated by ellipsometry with regard to the thickness of the layers compared to other literature [16]. Figure 1 illustrates Ellipsometry analysis based on the EMA thickness monitoring method, showing interference between the layers, (island structure of 10 nm Ag thin film, in sample A). For samples B and C, EMA thickness decreased significantly due to the uniform structure of the Ag thin film. This is achieved by both annealing the WO_3 thin film and increasing the thickness of the Ag thin film.

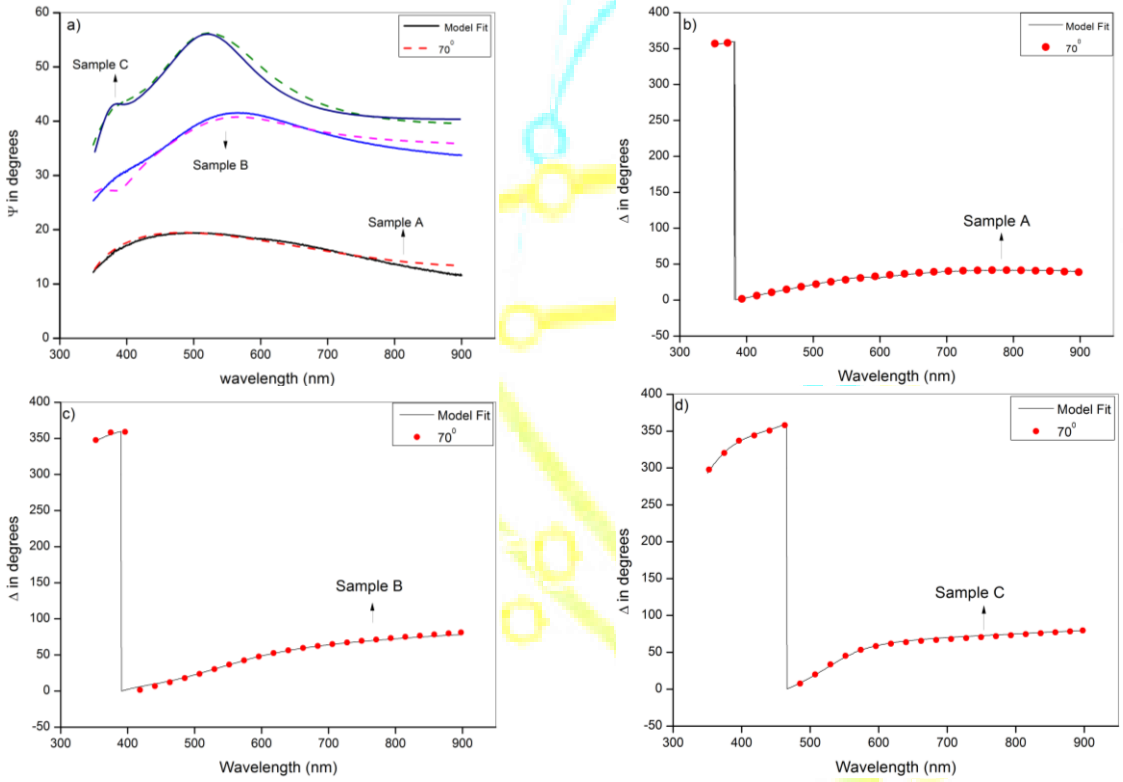

Fig. 1. a) Ψ Values for the experiment and model fit for sample A, B and C. b, c and d) Δ values for sample A, B and C, respectively.

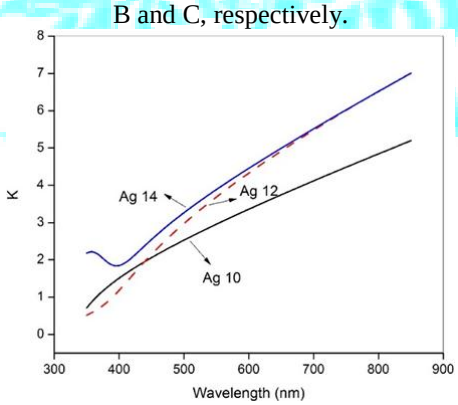

Fig. 2. Reliance of extinction coefficient of Ag film on its thickness.

Table 2. Thickness and MSE of the layers calculated in ellipsometry

Model Layers	WO_3 (Thickness) nm	EMA (Thickness) nm	Ag (Thickness) nm	EMA (Thickness) nm	WO_3 (Thickness) nm	MSE (nm)2
Sample A	39.5	7.11	0.86	3.25	37	0.5278
Sample B	40.05	0.3	10.9	0.4	39.90	1.2728
Sample C	39.80	0.43	13.90	0	40	1.0020

3.2. AFM analysis

Tungsten oxide in 40 nm of thickness deposited on the glass, then the film annealed at 300 ℃ for 1 hour. Variety of the films engineered and characterized by the appropriate analytical systems. AFM images and height histograms of the as deposited and annealed tungsten oxide with 40 mm thickness depicted in the Figs.3 (a, c) and 3 (b, d), respectively. Annealing at 300 ℃ for 1 hour in order to obtain a smoother surface executed. Comparing Fig.3c to 3d shows surface height distribution is narrower in annealed sample. Other annealing temperature and duration examined and undesirable surface morphology or dramatic decrease in transmittance perceived. Annealing is vital to rearrange the film structures. A decrease of 2.5 nm to 0.8 nm in roughness for as deposited and annealed film observed. Peak to peak value decreased sharply from 27.3 nm to 9.1 nm for as deposited and annealed film, respectively.

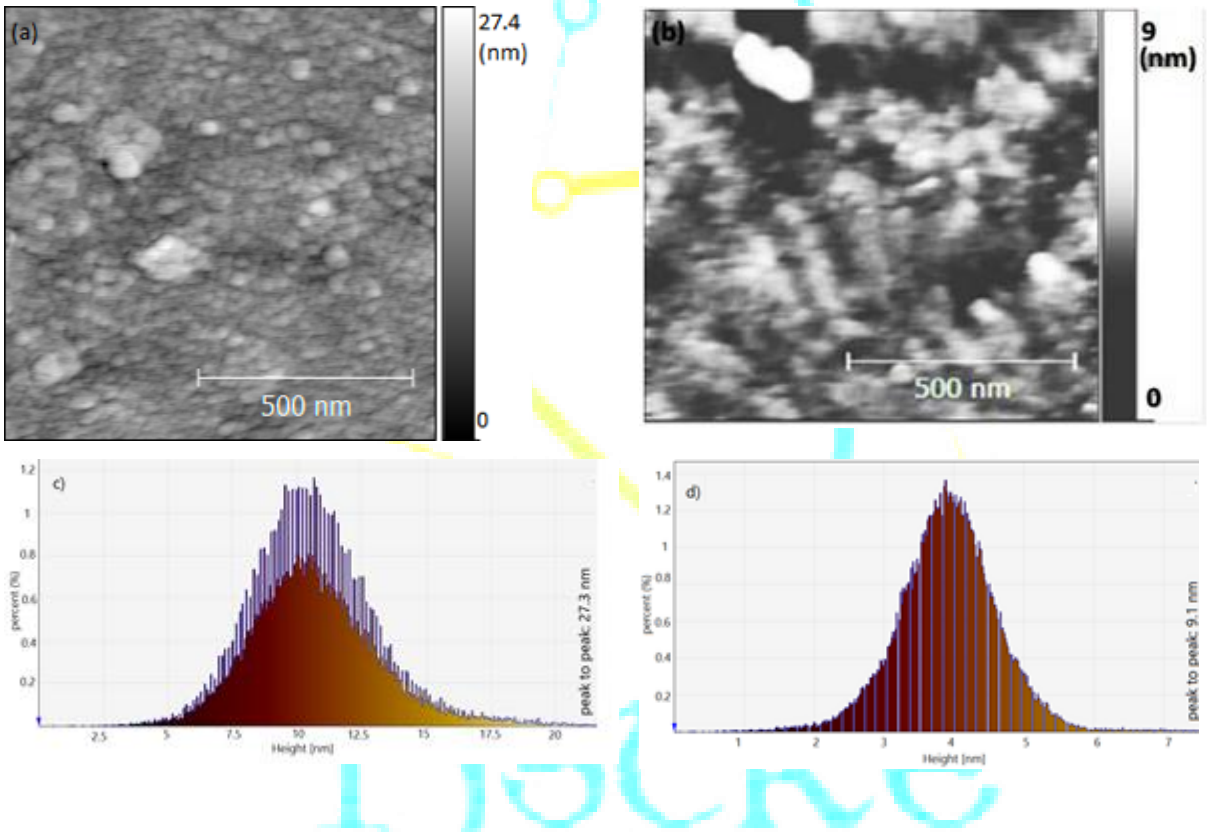

Fig. 3. Surface morphology from AFM topography: (a) 40 nm tungsten oxide as deposited on the glass (b) 40 nm tungsten oxide annealed at 300 ℃ for 1 hour (c-d) Height distribution of the 2D surface-height values from the respective AFM images.

Ag film deposited on the coated substrates with as deposited and annealed tungsten oxide layer. Figures 4a and 4b show the surfaces of 14nm Ag layer on the as deposited and annealed tungsten oxide films, respectively. Fig. 4b reveals that annealing tungsten oxide film and the thickness of Ag film, both are crucial in reducing the roughness of Ag film. Lower root mean square roughness (0.32 nm) and peak-to-peak surface height distribution (5.1 nm) observed in the latter compared to the former (rms roughness=1.9nm and peak-to-peak=17 nm).

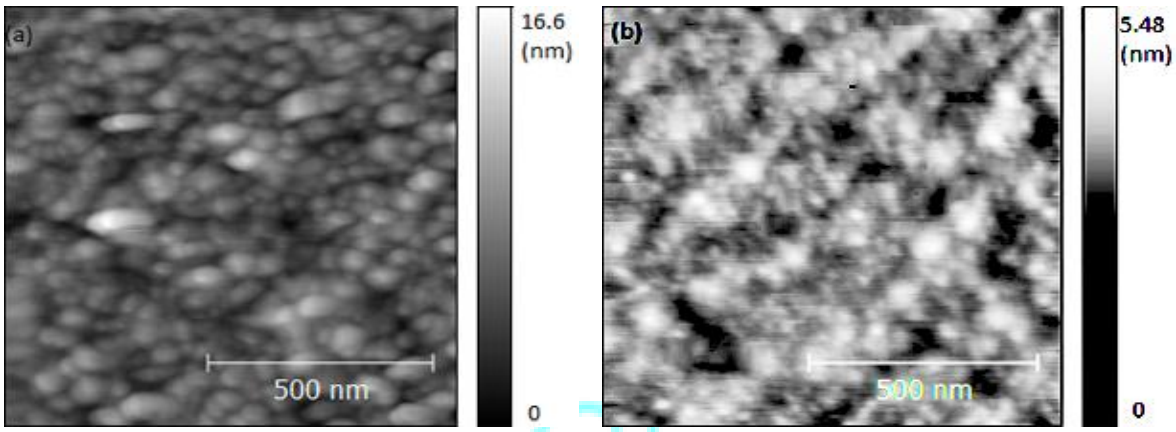

Fig. 2. AFM images of the 14 nm Ag films deposited on as deposited tungsten oxide (a) and annealed tungsten oxide (b) at room temperature.

3.3. Optical transmittance

The optical transmittance spectra of the WO_3/Ag/WO_3 (WAW) multilayer films with different Ag thin film thicknesses are shown in Figure 5. Samples A, B and C represent multipliers which fabricated simultaneously with samples A_1, B_1 and C_1 but annealing did not carry out on their first WO_3 layer. In Figure 5a, silver with 10 nm thickness did not show the selectivity which is needed for the heat mirrors. Figure 5b comparing the transmittance for two systems with 12 nm of silver thickness B_1 and B. Figure 5c illustrates the transmittance for the sample with 14 nm silver film thickness.

The transmittance patterns provide valuable information about the thicknesses of the silver layer on the heat mirrors performance. According to figure 5a silver with 10 nm thickness did not show the selectivity which is needed for the heat mirrors. This inability attributed to the island structure of silver layer resulted in scattering the incident light [6]. When the thickness of the silver layer increased, the selectivity improved. As it is evident from Fig. 5b, for 12nmthickness of Ag the transmittance of WAW films changed from 86% for as-deposited to more than 90% for annealed sample at 300℃. Decreased transmittance 41/5% and 50% are evident for annealed and as-deposited samples at λ=1100 nm, respectively. Finally, the transmittance of WAW films for 14nm Ag thickness varied from 91% for as-deposited to more than 94% for annealed sample at 300℃ in the wavelength of 550 nm. Decreased transmittance of 27.7% and 27.6% are observed for annealed and as-deposited samples at λ=1100 nm, respectively. It is evident that depart from thickness of Ag thin film, annealing the first WO_3 layer improved all the samples in terms of transparency in the visible region.

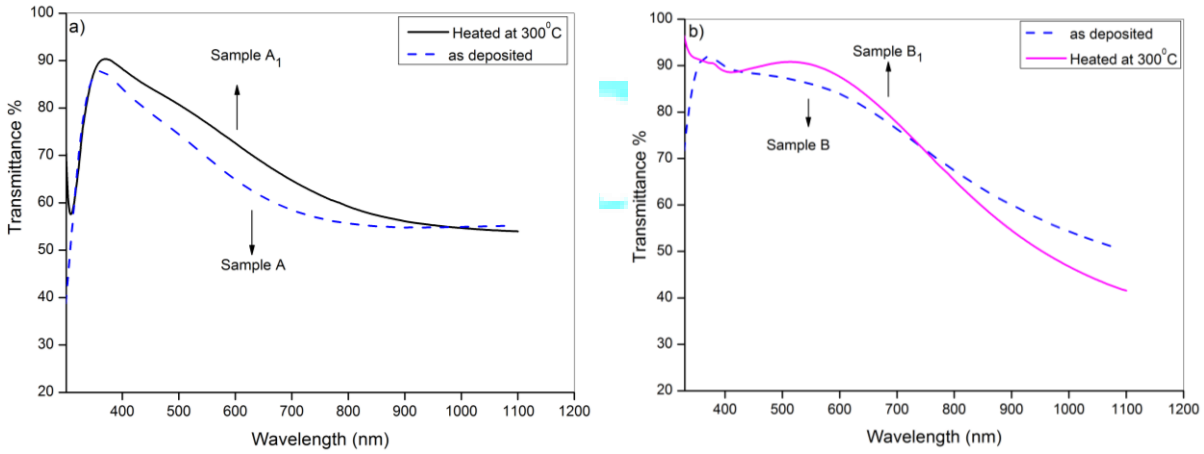

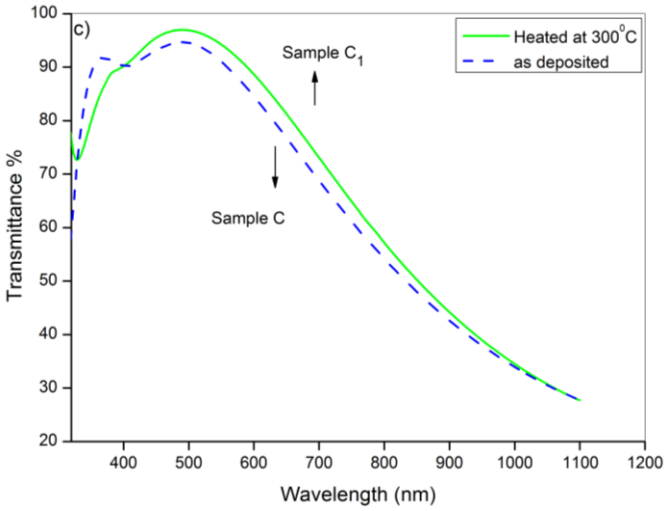

Fig. 5. Transmission measured as a function of wavelength for WO_3/Ag/WO_3 thin films deposited on glass. WO_3 film fixed at 40 nm and Ag thickness varied a)10 nm, b)12 nm, c)14 nm.

IV. Conclusion

The WO_3/Ag/WO_3 heat mirrors fabricated and the effect of annealing on the first layer WO_3 deposited film investigated. The study carried out on thickness variations of Ag film in the range 10-14 nm. While Ag deposited at fixed 40 nm thickness of WO_3 based on as deposited and annealed forms. Multilayer WAW films with 10 nm silver thickness did not exhibit the selectivity that needed for the heat mirrors. Ag film grown on annealed WO_3 significantly smoother and more uniform than developed in the as deposited WO3 film. Ellipsometry analyses confirm, there is almost no interfering between the layers in the sample with 12 and 14 nm Ag film deposited on the annealed WO_3 layer. Consequently, the effective thickness of the layers increases and improves optical performance. The best performance accomplished by 14 nm Ag film on annealed WO_3. The transmittance at λ =550 nm for the annealed sample raised about 3% and reached to 94% the highest reported for heat mirrors. This study showed that not only annealing is vital to form sharp layers, but also it has a crucial influence on the heat mirror performance.

References

[1] R. Groth and W. Reichelt, "Gold coated glass in the building industry" Gold Bull. **Vol.7 (3)**, 62-68 (1974).

[2] R. Groth and E. Kauer, "Thermal insulation of sodium lamps", Philips Tech. Rev. **26**, 105-111 (1965).

[3] D.Jafrancesco, P.Sansoni, F.Francini, G.Contento, C.Cancro, C.Privato, G.Graditi, D.Ferruzzi, L.Mercatelli, E.Sani, D.Fontani, "Mirrors array for a solar furnace: Optical analysis and simulation results" , Renewable Energy, **63**, Pages 263-271, (2014).

[4] G. Kokogiannakis J. Darkwa C. Aloisio, Simulating Thermochromic and Heat Mirror Glazing Systems in Hot and Cold Climates, Energy Procedia, **62**, 22-31 (2014).

[5] E. Matsubara, M. Nagaai, and M. Ashida, Coherent infrared spectroscopy system from terahertz to near infrared using air plasma produced by 10-fs pulses, J. Opt. Soc. Am B **30**, Issue 6, 1627-1630 (2013)

[6] J. Domaradzki, D. Kaczmarek, M. Mazur, D. Wojcieszak, J. Halarewicz, S. Glodek, P. Domanowski, Investigations of optical and surface properties of Ag single thin film coating as semitransparent heat reflective mirror, Materials Science-Poland, **34,** 747–753 (2016).

[7] H.A. Macleod, Multilayer High-Reflectance Coatings, Thin-Film Optical Filters, Fourth Edition, CRC Press, pp. 209-239 (2010).

[8] C.G. Granqvist, Transparent conductors as solar energy materials: A panoramic review, Solar Energy Materials and Solar Cells, **91**, 1529-1598 (2007).

[9] T. Andersson, C.G. Granqvist, Morphology and size distributions of islands in discontinuous films, Journal of Applied Physics, **48**, 1673-1679 (1977).

[10] Z. Wang, X. Cai, Q. Chen, L. Li, Optical properties of metal-dielectric multilayers in the near UV region, Vacuum, **80**, 438-443 (2006).

[11] B. Karlsson, E. Valkonen, T. Karlsson, C.G. Ribbing, Materials for solar-transmitting heat-reflecting coatings, Thin Solid Films, **86**, 91-98 (1981).

[12] H. S. So S. B. Hwang D. H. Jung H. Lee, Optical and electrical properties of Sn-doped ZnO thin films studied via spectroscopic ellipsometry and hall effect measurements, Journal of the Korean Physical

Society, **Vol.70,No.7,** 706-713 (2017).

[13] G.E. Jellison, F.A. Modine, Parameterization of the optical functions of amorphous materials in the interband region, Applied Physics Letters, **69** 371-373 (1996).

[14] G.B. Smith, G.A. Niklasson, J.S.E.M. Svensson, C.G. Granqvist, Noble-metal-based transparent infrared reflectors: Experiments and theoretical analyses for very thin gold films, Journal of Applied Physics, **59**, 571-581 (1986).

[15] I. Valyukh, S. Green, H. Arwin, G.A. Niklasson, E. Wäckelgård, C.G. Granqvist, Spectroscopic ellipsometry characterization of electrochromic tungsten oxide and nickel oxide thin films made by sputter deposition, Solar Energy Materials and Solar Cells, **94**, 724-732 (2010).

[16] M. M. Hasan, A. B. M. Abdul Malek, A. S. M. A. Haseeb and H. H. Masjuki, Investigations on tio2and ag based singleand multilayer films for window glazings, ARPN Journal of Engineering and Applied Sciences **Vol. 5,NO. 9,** 22-29 (2010).

[17] B.J. Malin, B. Gustavo, V. Iryna, P. Clas, A. Hans, A.N. Gunnar, Ö. Lars, Electronic and optical properties of nanocrystalline WO 3 thin films studied by optical spectroscopy and density functional calculations, Journal of Physics: Condensed Matter, **25,** 205502 (2013).